Computational Modeling of Carbonaceous Mesophase Rheology

Arvinder P. Singh and Alejandro D. Rey
Chemical Engineering Department, McGill University
3610 University Street, Montreal, Quebec H3A 2B2 CANADA

Carbonaceous mesophases (CMs) or discotic mesophases are precursor materials used in the manufacturing of high performance carbon fibers that possess high stiffness and thermal conductivity. There has been a great interest in understanding the texture evolution during the fiber formation melt spinning process in which the CMs are subjected to non-homogeneous mixed shear and extensional flows. In this work we present the microstructural response of model CMs under rectilinear shear flows, and thereby identify and characterize the novel relations among rheology, microstructure and processing conditions. The simulations are used to put forth the fundamental principles that govern fiber texture generation under shear.

Theory and Governing Equations

The evolution of microstructure, in terms of the tensor order parameter $\mathbf{Q}(y, t)$, in discotic mesophases under shear flows is governed by the following constitutive equation:

$$\frac{d\mathbf{Q}}{dt}=[\mathbf{W}\cdot\mathbf{Q}-\mathbf{Q}\cdot\mathbf{W}+\tfrac{2}{3}\beta\mathbf{A}+\beta[\mathbf{A}\cdot\mathbf{Q}+\mathbf{Q}\cdot\mathbf{A}-\tfrac{2}{3}(\mathbf{A}:\mathbf{Q})\mathbf{I}] \quad (1)$$
$$-\tfrac{1}{2}\beta[(\mathbf{A}:\mathbf{Q})\mathbf{Q}+\mathbf{A}\cdot\mathbf{Q}\cdot\mathbf{Q}+\mathbf{Q}\cdot\mathbf{A}\cdot\mathbf{Q}+\mathbf{Q}\cdot\mathbf{Q}\cdot\mathbf{A}-\{(\mathbf{Q}\cdot\mathbf{Q})\mathbf{A}\}\mathbf{I}]]$$
$$-\frac{1}{Pe}\frac{6}{(1-\frac{3}{2}\mathbf{Q}:\mathbf{Q})^2}[(1-\tfrac{1}{3}U)\mathbf{Q}-U\mathbf{Q}\cdot\mathbf{Q}+U\{(\mathbf{Q}:\mathbf{Q})\mathbf{Q}+\tfrac{1}{3}(\mathbf{Q}:\mathbf{Q})\mathbf{I}\}]$$
$$+\frac{1}{Er}\frac{1}{(1-\frac{3}{2}\mathbf{Q}:\mathbf{Q})^2}\left[\nabla^2\mathbf{Q}+\frac{L_2}{2L_1}\left[\nabla(\nabla\cdot\mathbf{Q})+\{\nabla(\nabla\cdot\mathbf{Q})\}^T-\tfrac{2}{3}\mathrm{tr}\{\nabla(\nabla\cdot\mathbf{Q})\}\mathbf{I}\right]\right]$$

The above set of equations (1) accounts for viscous effects, short range homogeneous elasticity and long range curvature elasticity. There are two dimensionless numbers: *Pe* and *Er* representing ratio of viscous flow effects to short range order elasticity effects, and ratio of viscous flow effects to long range order elasticity effects respectively. **A**, **W**, U, β are the dimensionless vorticity tensor, dimensionless rate of deformation tensor, nematic potential and shape factor respectively. For details see [1].

In this work fixed boundary conditions are used, such that the director **n** is anchored along vorticity direction (z-axis) at the bottom stationary plate, and along the velocity gradient direction (y-axis) on the top moving plate, see Figure 1. The director orientation is characterized by a polar (out-of-plane) angle ϕ and an azimuthal (in-plane) angle θ. This set of BCs corresponds to the anchoring conditions in a HAN cell. Both BCs are along the stable attractors for model CMs under homogeneous shear flows [1]. In the present work the parametric values are set at U = 6, β = -0.9, L_2/L_1 = -4/3. The simulations are performed for the ranges $0.1 \le Pe \le 500$ and $0 \le Er \le 5000$.

Numerical Results and Discussion

An extensive computational investigation of the governing equation (1) has been performed. The microstructure features of model CMs are characterized by one time dependent periodic and two steady states. A brief description of the relevant features of these three regimes is given below:

1. Elastic-Driven Steady State (ESS)

This stable steady state appears at low *Pe* for all *Er*, and prevails when the long range elastic effects dominate and quench the vorticity effects due to flow. Figure 2 shows the director Polar angle ϕ as a function of non dimensional gap (y/H) between the plates for *Pe* = 10, and *Er* = 100 (solid line), 1000 (dashed line). At low *Er* the out of plane angle changes monotonically from bottom plate to top plate, however, at high *Er* the director aligns near the vorticity axis in most of the domain ($0<y/H<0.75$), and decreases sharply near the top plate. The long range elasticity effects are stronger at lower *Er* (*Er*=100) thereby maintaining lower spatial gradients than at higher *Er* (*Er*=1000). In this regime the uniaxial (biaxial) $S(P)$ scalar order parameters are near their equilibrium values. The inset schematics represent the corresponding fiber textures discussed below.

The main features of the ESS regime are: (a) the orientation field reaches steady state; (b) the steady state arises due to long range elasticity, (c) the nematic phase is mostly uniaxial.

2. Composite Kayaking-Limit Cycle Periodic State (KLS)

This periodic state appears at sufficiently high *Er* and for intermediate range of *Pe*. Figure 3 shows (a) uniaxial (S) and (b) biaxial (P) scalar order parameter as a function of dimensionless time (t) and distance (y/H) for *Er* =1000 and *Pe* = 50. The director dynamics are rotational, and the scalar order parameters (S, P) oscillate with the nucleation of an abnormal nematic state in the bulk (at $y^* = y/H \approx 0.84$ in this case). As *Pe* increases the nucleation point moves away from the top plate towards the lower plate. The director rotates in kayaking orbits in the region $0<y/H<y^*$, and in out-of-plane limit cycles in the rest of the domain $y^*<y/H<1$, as shown in Fig. 3(c). In a kayaking orbit the director rotates clockwise in a closed loop, which extends (shrinks) towards the velocity gradient (flow) direction, around the vorticity axis in which it slows down near the velocity gradient direction. For more details see [1]. In limit a limit cycle the director trajectories too make a closed loop that is eccentric to the vorticity axis. The

kayaking and limit cycle orbits shrinks as we move close to the walls. The abnormal nematic states nucleate where the kayaking orbits and the limit cycle merge.

The salient features of this periodic state are: (a) the director dynamics in the bulk are rotational and correspond to kayaking orbits near the bottom plate and to limit cycles near the top plate, (b) at the boundary between these two regions abnormal nematic states nucleate, (c) the abnormal nematic states emerge in the bulk.

3. Viscous Driven Steady State (VSS)

This steady state appears at sufficiently high Er and at appropriate Pe. This steady state arises due to the dominance of viscous flow over short and long range elasticity. Figure 4 shows the director polar angle ϕ profiles at VSS as a function of non-dimensional gap (y/H) for Er = 100, and Pe = 100 (solid line), 1000 (dash triple-dot line), and for Er = 1000, Pe = 100 (dashed line). The bulk orientation in the region $y/H<\delta_c$ is along the vorticity axis ($\phi = 90$), and that in the region $y/H>\delta_c$ is in plane, and along the velocity gradient direction ($\phi = 0$, $\theta = 90$). The sharp director reorientation in the bulk is compensated by a corresponding sharp dip (spike) in bulk alignment S (P). δ_c increases with increasing Pe, and decreases with Er as shown in Fig. 4.

The main features of the VSS regime are: (a) the orientation field reaches a steady state; (b) the steady state arises due to viscous flow, (c) discontinuity in the director orientation field, and (d) nematic phase is highly biaxial.

Implications of Numerical Results on Fiber Textures

It is shown in [2] that the pure radial (onion) fiber texture is consistent with director orientation along vorticity (velocity gradient) direction. Using the same reasoning, we find that the director orientation in VSS corresponds to a mixed texture with radial core and onion exterior, shown in Fig. 4. The size of radial core δ_c is a function of Pe and Er as mentioned above. The director orientation in ESS at high Er (Er=1000) corresponds to a texture with a fairly large radial core with folded outer layers, see Fig. 2. At lower Er (Er=100) the continuos decrease in out-of-plane director orientation results in a folded texture morphology, in which a small inner radial core is connected smoothly with the outermost onion layer, as shown in Fig. 2. The presented model also predicts the textures with onion core.

Acknowledgment is made to the Donors of Petroleum Research Fund, administered by American Chemical Society, for support of this research

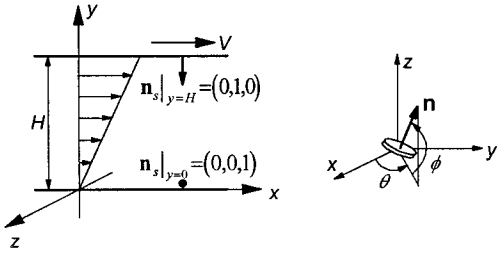

Figure 1: Definition of flow geometry, coordinate system and boundary conditions.

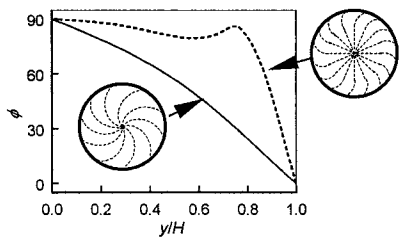

Figure 2: Director polar angle ϕ as a function of non-dimensional gap (y/H) between the plates for Pe = 10, and Er = 100 (solid line), and 1000 (dashed line). The inset schematics represent the corresponding fiber textures.

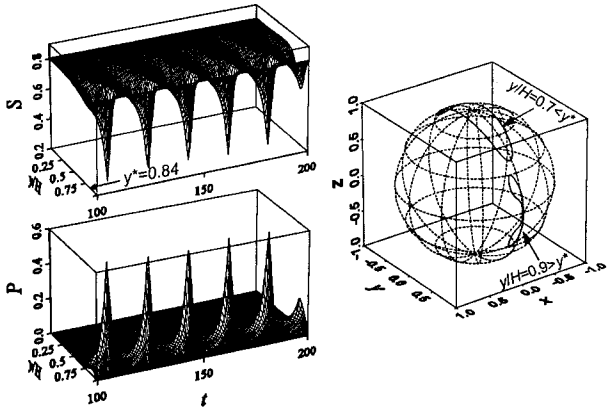

Figure 3: Uniaxial (S) and biaxial (P) scalar order parameter as a function of dimensionless time (t) and gap (y/H) for Er =1000 and Pe = 50. Director profiles on unit sphere at y/H = 0.7 (kayaking orbit) and y/H = 0.9 (limit cycle). Abnormal nematics appear at $y^* \approx 0.84$.

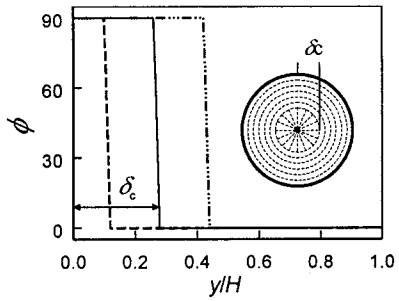

Figure 4: Director Polar angle ϕ as a function of non dimensional gap (y/H) between the plates for Er = 100, and Pe = 100 (solid line), 1000 (dash triple-dot line), Er = 1000, and Pe = 100 (dashed line).

References

[1] Singh AP, Rey AD. Microstructure constitutive equation for discotic nematic liquid crystalline materials, Part I: Selection procedure and shear flow predictions. Rheo Acta 1998;37(1):30-45.

[2] Singh AP, Rey AD. Consistency of predicted shear-induced orientation modes with observed mesophase pitch-based carbon fiber textures. Carbon 1998;36(12):1855-1859.